Solvent-Dependent Stabilization of Gold Nanoparticles: A Comparative Study on Polymers and the Influence of Their Molecular Weight in Water and Ethanol

Marilyn Kaul , Rolf Lennart Vanselow , Ahmed Y. Sanin , Ulf D. Kahlert , Christoph Janiak *

Posted Date: 13 August 2025

doi: 10.20944/preprints202508.0950.v1

Keywords: gold nanoparticles; nanoparticle synthesis; polymer coating; stability; solvent

 doi:10.20944/preprints202508.0950.v1

Article

Solvent-Dependent Stabilization of Gold Nanoparticles: A Comparative Study on Polymers and the Influence of Their Molecular Weight in Water and Ethanol

Marilyn Kaul [1], Rolf Lennart Vanselow [1], Ahmed Y. Sanin [2], Ulf D. Kahlert [2] and Christoph Janiak [1,*]

[1] Institute for Inorganic and Structural Chemistry, Heinrich-Heine-University Düsseldorf, 40204 Düsseldorf, Germany

[2] Molecular and Experimental Surgery, University Clinic for General-, Visceral-, Vascular- and Transplant Surgery, Faculty of Medicine, Otto-von-Guericke-University Magdeburg, 39120 Magdeburg, Germany

* Correspondence: janiak@uni-duesseldorf.de; Tel.: +49-211-81-12286

Abstract

Gold nanoparticles (AuNPs) are attracting more and more attention in life sciences, especially due to their versatile physicochemical properties. They are biocompatible, air and water stable and easy to synthesize. Yet, the colloidal stability of AuNPs not only in water but also in organic solvents remains a decisive factor for their practical usage. This study therefore investigated the influence of different polymer coating methods and polymer types using the postsynthetic addition reaction (PAR) and the one-pot synthesis with the polymers poly(vinyl alcohol) (PVA), poly(ethylene glycol) (PEG), poly(vinylpyrrolidone) (PVP) and poly(acrylic acid) (PAA) each with different molar weight averages. Analysis of the AuNP@Polymer conjugates by transmission electron microscopy (TEM) finds essentially unchanged gold nanoparticle core sizes of 11-18 or 11-19 nm in water and ethanol, respectively. The hydrodynamic diameter from dynamic light scattering (DLS), which also includes the polymer shell, lies largely in the range from 20-70 nm and ultraviolet-visible spectroscopy (UV-Vis) showed gold plasmon resonance band maxima between 517-531 nm over both synthesis methods and solvents for most samples. The polymer PVA showed the best colloidal stability in both synthesis methods, both in water and after transfer to ethanol, and thus provides the best protection for the AuNPs against aggregation. An increased instability in ethanol could only be noted for the PEG coated samples apparently due to the less-coordinating ether groups of the polymer. For the polymers PVP and PAA the stability depended more specifically on the combination of synthesis method, polymer molecular weight and solvent.

Keywords: gold nanoparticles; nanoparticle synthesis; polymer coating; stability; solvent

1. Introduction

Gold nanoparticles (AuNPs) are becoming increasingly popular due to their unique physical, chemical and optical properties and are being used more and more frequently in medicine [1,2]. The synthesis of AuNPs is simple, they are biocompatible, air and water stable, the size and shape are easy to vary, they can be formulated with high solubility in water and they can be loaded with drugs or antibodies [3–6]. AuNPs exhibit a characteristic surface plasmon resonance (SPR), which typically occurs at around 520 nm for AuNPs synthesized with sodium citrate (NaCit) [7]. In colloidal form, this results in their reddish color. SPR is sensitive to various physicochemical parameters such as particle size, shape, environment, and aggregation state, thereby enabling targeted control of optical

 doi:10.20944/preprints202508.0950.v1

properties. The aggregation of AuNPs leads to a shift in SPR and color change from red to blue, which can be used as a simple, visual indicator of instability or interactions in the solution [8].

Due to their easy modification, they offer an exciting field of application as carrier materials for therapeutic or diagnostic agents [9,10]. The targeted control of size, shape, monodispersity and surface functionalization of gold nanoparticles (AuNPs) plays a central role in their successful use in nanomedicine. Numerous recent studies show that these physicochemical properties significantly influence the behavior, efficacy, colloidal stability, and dispersibility of AuNPs in various solvents [11].

However, a key challenge and an important prerequisite for the use of AuNPs is to ensure that they are monodisperse and highly stable, especially when environmental parameters like the solvent are changed. For certain biomedical applications, it is necessary for AuNPs to remain well dispersed and stable in both water and organic solvents such as ethanol. A loss of stability and the subsequent associated aggregation usually leads to a loss of function of the AuNPs [12]. For example, some active pharmaceutical ingredients are only soluble in organic solvents and for their loading onto the AuNPs, the latter must be stable in the organic medium [13]. The surface-coating of the AuNPs is fundamental for the AuNP stability towards variations in solvents, over time or further functionalization [14,15].

A non-optimal coating for the given conditions and time leads to reduced colloidal stability of the AuNPs, which results in agglomeration and subsequent deterioration of the desired properties of the nanoparticles, thus limiting their practical applicability. Therefore, maintaining the colloidal stability of AuNPs in aqueous and organic environments is often crucial for their practical use [16]. Furthermore, spherical gold nanoparticles should be aimed for as non-spherical particles are more prone to agglomeration due to their curvature [17]. A knowledge and comparison of different polymer-based stabilization and optimized synthesis methods is crucial to prepare stable AuNPs and to avoid unwanted agglomeration with loss of functionality. Albanese et al. showed that aggregated AuNPs can exhibit a lower cell uptake than monodisperse AuNPs [18]. Cell uptake also decreases for rod-shaped NPs compared to spherical AuNPs. This is because rod-shaped NPs require more time to be completely enclosed by the cell membrane [19]. Therefore, various synthesis strategies and polymer-based surface coatings have been developed. Polymers such as poly(vinyl alcohol) (PVA), poly(ethylene glycol) (PEG), poly(vinylpyrrolidone) (PVP) and poly(acrylic acid) (PAA) act as effective steric and electrostatic stabilizers [11]. The use of these polymers represents a promising approach for AuNP stabilization, as they form a protective shell around the AuNPs, minimizing particle-to-particle interactions and biofouling and increasing resistance to solvent changes [17,20,21].

PEG is one of the most commonly used biopolymers for the steric stabilization of AuNPs in nanomedicine, which is also termed PEGylation [22,23]. PEG is thought to form a protective barrier around the nanoparticles to prevent their agglomeration, increase the biocompatibility of the AuNPs, prolong their circulation time in the blood, and to prevent them from being marked by the immune system and rapidly degraded [24–27]. According to reports, higher molecular weight PEG (5000 Da) coated AuNPs are more stable than lower molecular weight PEG (2000 Da) coated AuNPs in water [22].

In addition to stabilization in water and ethanol, polymer coatings enable targeted control of particle size and surface chemistry, which is relevant for other applications such as the deposition and the cell uptake of an active ingredient (Figure 1). The active ingredient can be embedded in the polymer shell through supramolecular interactions with the polymers, which is advantageous as the chemical structure of the active ingredient remains unchanged, thus avoiding unexpected or unwanted reactions [11].

Through endocytosis, the AuNPs can enter the cell by interacting with the plasma membrane or the extracellular matrix. In endocytosis, AuNPs are taken up by invaginations of the cell membrane. These invaginations then constrict and form small vesicles that transport the NPs into the cell interior, this enables delivery of the active ingredient into a cell. Shan et al. reported that AuNPs ranging in size from 4 to 17 nm were endocytosed in cells under native conditions [28,29]. The accumulation of AuNPs in tumor tissue occurs via the so-called enhanced permeability and retention (EPR) effect.

 doi:10.20944/preprints202508.0950.v1

Tumor vessels have significantly larger and more permeable blood vessels (200 nm to 1.2 µm) than normal blood vessels (<10 nm), which means that AuNPs preferentially accumulate in tumor tissue [11,30,31], enabling increased drug delivery to tumor tissue without the need for specific target ligands. Internal stimuli such as pH changes or external stimuli such as heat or light can trigger and additionally enhance the release of the active substance from the AuNP surface [32].

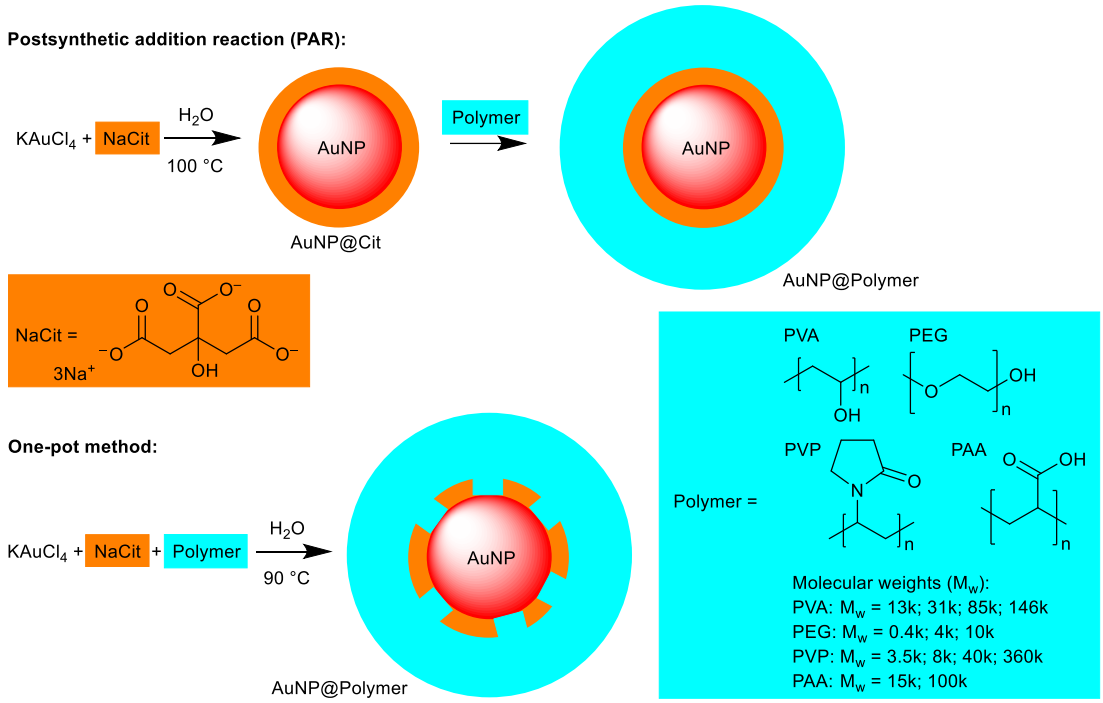

Figure 1. Schematic illustration of the AuNP synthesis methods and the polymers used for the AuNP@Polymer conjugates.

The aim of this work was to produce gold-polymer conjugates that remain stable after exchanging the solvent from water to ethanol. For this purpose, different biocompatible polymers with different molar weight averages and functional groups were used. The polymers were applied during the formation of the AuNPs in a postsynthetic addition reaction (PAR) and in a one-pot reaction to preformed Au-citrate nanoparticles.

2. Materials and Methods

2.1. Materials

Potassium tetrachloridoaurate(III) ($KAuCl_4$), Polyvinyl alcohol (PVA) $M_w \sim 13\,000$ g/mol, 31 000 g/mol, 85 000 g/mol, 146 000 g/mol, Polyethylene glycol (PEG) $M_w \sim 400$ g/mol, Polyvinylpyrrolidone (PVP) $M_w \sim 3500$ g/mol, 360 000, Poly(acrylic acid) $M_w \sim 15\,000$ g/mol and 100 000 were ordered from Sigma Aldrich, Darmstadt, Germany. PEG $M_w \sim 10\,000$ g/mol, PVP $M_w \sim 8\,000$ g/mol were from Across Organics, Thermo Fisher Scientific, Schwerte, Germany. PEG $M_w \sim 4000$ g/mol was purchased from JK Chemicals, Vapi, India and PVP $M_w \sim 40\,000$ g/mol was supplied from TCI, Eschborn, Germany. Sodium citrate dihydrate (NaCit) was from J.T. Baker Chemicals, Schwerte, Germany. Dasatinib (DASA) was obtained from BLD Pharmatech GmbH, Kaiserslautern, Germany. Ethanol with p.a. purity were from Merck, Darmstadt, Germany.

All materials were commercially available and were used without further purification. Ultrapure water obtained from an Arium Mini® system from Sartorius was used for the AuNPs synthesis.

 doi:10.20944/preprints202508.0950.v1

2.2. Characterization Methods

Centrifuge: The samples were centrifuge using the Sigma 3-30KHS from Sigma. All centrifugation steps were performed at the specified parameters of the relative centrifugal force of 10,464 × g, a time of 20 min, at a temperature of 4 °C, where g corresponds to the Earth's gravitational force of 9.81 m/s^2. The elative centrifugal force (rcf) is expressed as a multiple of the Earth's gravitational force measurement for a standardized centrifugation protocol as the force applied to a sample during centrifugation.

Transmission electron microscopy (TEM): TEM images were recorded with a JEOL JEM-2100Plus electron microscope at an accelerating voltage of 200 kV with a Matataki Flash camera. The size of the AuNPs were measured with a GatanDigital Micrograph software and over 200 particles were counted for the size distribution. Each AuNP solution was diluted by adding 20 µL of the AuNP sample to either 80 µL of water, for the water samples, or 80 µL of ethanol, for the ethanol samples. 10 µL of the diluted dispersion was dropped onto a 200 µm carbon-coated copper grid from Electron Microscopy Sciences (Munich, Germany). The grid with the solution was dried at ambient conditions (~20 °C, ~50% relative humidity) and stored at ambient conditions in closed vials under air until the measurement.

Dynamic light scattering (DLS): Hydrodynamic diameters and the polydispersity index (PDI) were recorded with a Malvern Nano S Zetasizer with a HeNe laser at a wavelength of 633 nm.

Ultraviolet-visible (UV-Vis): UV-Vis spectra were determined on a P9 double beam spectrophotometer from VWR.

High-performance liquid chromatography (HPLC): The DASA concentration before and after loading was determined on a Shimadzu LC 20AT instrument with an SPD-M20A UV-Vis detector and a Luna C18(2) (250 × 4.60 mm, 5 micron) column from Phenomenex®. The samples were filtered through a 0.2 µm Millex filter from Millipore® and all solvents used were degassed with the ultrasonic bath (Bandelin Sonorex, Berlin, Germany) before use. The mobile phase consisted of methanol-water (82:18, v/v) and had a flow-rate of 1 mL min^{-1} at room temperature. The detector wavelength was set to 322 nm and the injection volume was 20 µL.

2.3. Synthesis of Polymer Stabilized Gold Nanoparticles (AuNP@Polymer) in Water

2.3.1. Postsynthetic Addition Reaction

In a 500 mL Erlenmeyer flask with a glass stopper, a total of 20 mg (52.9 µmol) of $KAuCl_4$ was dispersed in 200 mL ultrapure water and heated to 100 °C. 90 mg (350 µmol) of sodium citrate dihydrate (NaCit) was then added and the solution was heated to 100 °C for a further 15 minutes. During this time, the color solution turns from light yellow to dark red. Finally, the solution was cooled to room temperature, 4.3 µmol of polymer was added and stirring continues for 12 h. The DLS and UV-Vis measurements were taken directly after the 12 h. The DLS measurements were taken without dilution, and for the UV-Vis measurements, the solution was diluted with water in a ratio of 50:50. The remaining AuNP solutions were stored in the refrigerator at 4 °C in the reaction flask.

2.3.2. One-Pot Synthesis

In a 500 mL round bottom flask the amount of 20 mg (52.9 µmol) of $KAuCl_4$ and 4.3 µmol of polymer were dissolved in 200 mL of ultrapure water and the solution was heated to 90 °C under stirring. At 90 °C, 90 mg (350 µmol) of NaCit was added and the solution was continued to stir for 30 min. The color changed from light yellow to dark red. The DLS and UV-Vis measurements were taken directly after cooling to room temperature and were measured as described in section 2.3.1 above. The remaining AuNP solutions were stored in the refrigerator at 4 °C in the reaction flask.

2.4. Transfer of Polymer Stabilized Gold Nanoparticles (AuNP@Polymer) from Water to Ethanol

From the aqueous dispersion, 5 mL were centrifuged, the supernatant water was separated by decantation and discarded and the AuNP@Polymer precipitate was resuspended in 5 mL of ethanol.

 doi:10.20944/preprints202508.0950.v1

The DLS and UV-Vis measurements were performed immediately afterwards. The solutions were measured in the DLS without dilution and the UV-Vis in a dilution of 50:50 (water:ethanol). The TEM grid and AuNP solutions storage were carried out as described above in section 2.3.1.

2.5. Loading of DASA on the AuNP@Polymer Conjugates

The AuNP@conjugate samples were transferred from water to ethanol as described in section 2.4. The 5 mL water or ethanol dispersion contains a gold mass mAu = 0.26 mg. From an ethanolic DASA stock solution (stored in refrigerator at 4 °C) with a concentration of 1 g/L, the volume of 0.8 mL (containing 0.8 mg DASA) was added to the 5 mL of the ethanolic AuNP@Polymer dispersion during stirring. The combined 5.8 mL of dispersion was stirred for further 72 h at ambient temperature. After 72 h the samples were centrifuged and the supernatants were stored in the refrigerator at 4 °C until the HPLC measurement to determine the remaining DASA concentration in order to obtain the adsorbed amount on the AuNP@Polymer conjugate from the difference.

3. Results and Discussion

3.1. Synthesis and Characterization of the AuNP Samples in Water

In this work, the ligand exchange reaction and the one-pot synthesis for the preparation of spherical AuNPs were investigated. In the two-step ligand exchange reaction the AuNPs are first synthesized with citrate (from sodium citrate) which has the dual role of a reductant of the Au(III) precursor as well as a stabilizing agent. Then in a second separate step another ligand or stabilizer is added to form the desired coating. Using this method, targeted surface modifications can be obtained and ligands can be used in the method that would not be suitable under the AuNP synthesis reaction conditions. However, a disadvantage of this method can be the incomplete replacement of the original citrate ligand layer. It is unclear if the citrate anion coating on the gold surface is indeed replaced by neutral polymer chains or rather, if the polymer wraps around the citrate-stabilized AuNP particles (AuNP@Cit). For this reason, here in this work we will refer to a PAR for the addition of the polymer instead of a ligand-exchange reaction. We note that in the literature the 'postsynthetic addition reaction' is referred to as 'ligand exchange reaction'. In the single-step one-pot synthesis the polymer is already present in the reaction mixture where the AuNPs are formed. Hence, the polymer coating can take place during the nucleation and growth steps. This seems advantageous, but can lead to a competition between stabilization and growth resulting in a larger variation of particle size [33–35].

The PAR consisted of first producing AuNP@Cit with the established Turkevich et al. method [36]. For this, $KAuCl_4$ was used as a gold precursor and sodium citrate as a reducing and stabilizing agent. Subsequently, the polymer was added to produce polymer-coated AuNPs. In the one-pot synthesis the gold precursor ($KAuCl_4$), the reducing agent (NaCit) and the polymer were added to the reaction vessel.

The four following polymers with different molar weight averages were used here to compare the stability of the AuNPs: poly(vinyl alcohol) (PVA) with the molar masses (M_W) of 13,000; 31,000; 85,000 and 146,000 g/mol, poly(ethylene glycol) (PEG) in the molar masses of 400; 4,000 and 10,000 g/mol, poly(vinylpyrrolidone) (PVP) in the molar masses of 3,500; 8,000; 40,000 and 360,000 g/mol and poly(acrylic acid) (PAA) in the molar masses of 15,000 and 100,000 g/mol. The polymers with their molar masses are in the following designated from PVA13k, PVA146k, over PEG0.4k, PEG10k, PVP3.5k, PVP360k to PAA15k and PAA100k.

For characterization of the AuNP@Polymer conjugates, transmission electron microscopy (TEM) provides a direct image of the gold cores of the conjugates with morphology, size, size distribution, dispersion or possible agglomeration, but does not visualize the size with the polymer. The TEM images of the AuNP@Polymer conjugates in water are shown in Figure 2 (PAR) and Figure 3 (one-pot), and Figure 4 provides a summarizing overview of the AuNP size. The corresponding size values are summarized in Table S1. The TEM images and the histograms in Figure 2 and Figure 3 reveal

 doi:10.20944/preprints202508.0950.v1

mostly spherical and monodisperse AuNP cores with an average size in-between 11-18 nm and a size-dispersion (σ) of mostly ± 1-2 nm. In the one-pot method, the polymers PVP and PAA15k did not result in well-separated, spherical AuNPs, but rather in anisotropic, elongated particles. However, with the polymer PAA100k, unusually small AuNPs were obtained in the one-pot method.

The comparison in Figure 4 illustrates that the one-pot synthesis gives largely a smaller average size of AuNPs than the PAR. This may show a stabilizing effect of the polymer when present during the nucleation of the AuNP leading to a slower growth rate resulting in the formation of many small nuclei rather than a few large particles [37]. However, there is no large difference between the two synthesis methods as the average size of the AuNPs lies overall in-between 11-18 nm and when the standard deviations are taken into account, the average size overlap. Noteworthy exceptions are PVP40k, PVP360k and PAA100k which give significantly smaller AuNPs in the one-pot synthesis.

With the one-pot route and the polymers PVA, PVP and PAA one can note that there are also smaller AuNPs formed with the longest polymer chains (highest molar mass). Polymers with a longer chain length increase the viscosity, which reduces the diffusion of the gold ions in the dispersion and this also slows down the growth rate which leads to smaller particles.

The gold core size dispersion for the two synthesis methods is also similar for PVA and PEG. Yet, with the polymers PVP and PAA the size dispersion increases for the one-pot over the PAR synthesis. Interestingly, with PVP and PAA the one-pot synthesis also produced non-spherical AuNPs which are considered disadvantageous as non-spherical particles are usually less stable. It is evident that the polymer functional groups, the chain length and mode of addition play a crucial role in determining the AuNP size, size dispersion and morphology.

For the synthesis of spherical AuNPs in water with sizes between 11-18 nm and with small size dispersion the PAR method could successfully be used with all polymers and chain lengths. The one-pot method, on the other hand, only leads to the formation of spherical particles independent of chain lengths for the polymers PVA and PEG but not with PVP and PAA.

 doi:10.20944/preprints202508.0950.v1

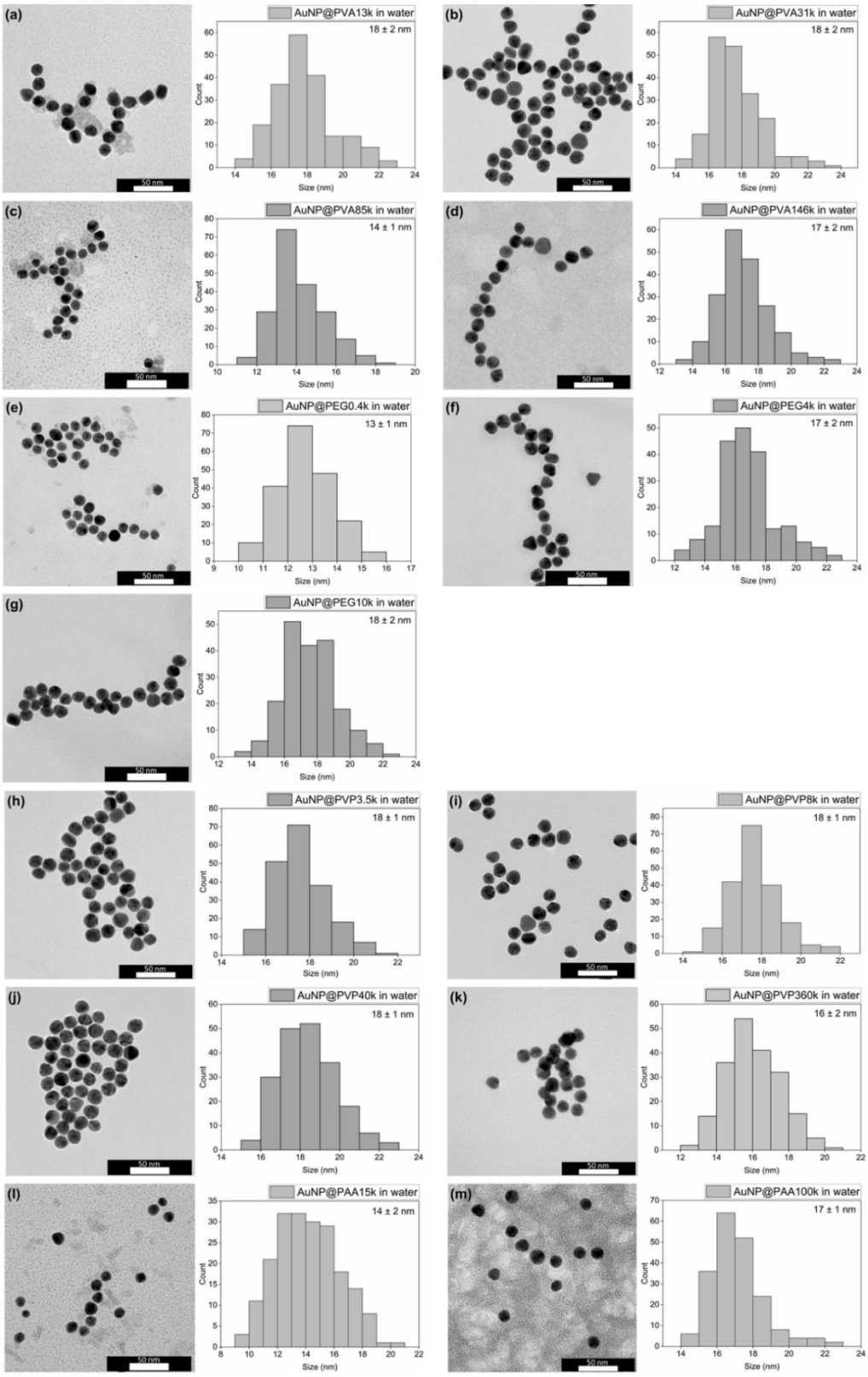

Figure 2. TEM images and histograms (with the average size and its standard deviation given) of the PAR synthesis in water of (**a**) AuNP@PVA13k (size = 18 ± 2 nm), (**b**) AuNP@PVA31k (18 ± 2 nm), (**c**) AuNP@PVA85k (14 ± 1 nm), (**d**) AuNP@PVA146k (17 ± 2 nm), (**e**) AuNP@PEG0.4k (13 ± 1 nm), (**f**) AuNP@PEG4k (17 ± 2 nm), (**g**) AuNP@PEG10k (18 ± 2 nm), (**h**) AuNP@PVP3.5k (18 ± 1 nm), (**i**) AuNP@PVP8k (18 ± 1 nm), (**j**) AuNP@PVP40k (18 ± 1 nm), (**k**) AuNP@PVP360k (16 ± 2 nm), (**l**) AuNP@PAA15k (14 ± 2 nm) and (**m**) AuNP@PAA100k (17 ± 1 nm). For the histograms 200 particles were analyzed using larger areas of the TEM images.

 doi:10.20944/preprints202508.0950.v1

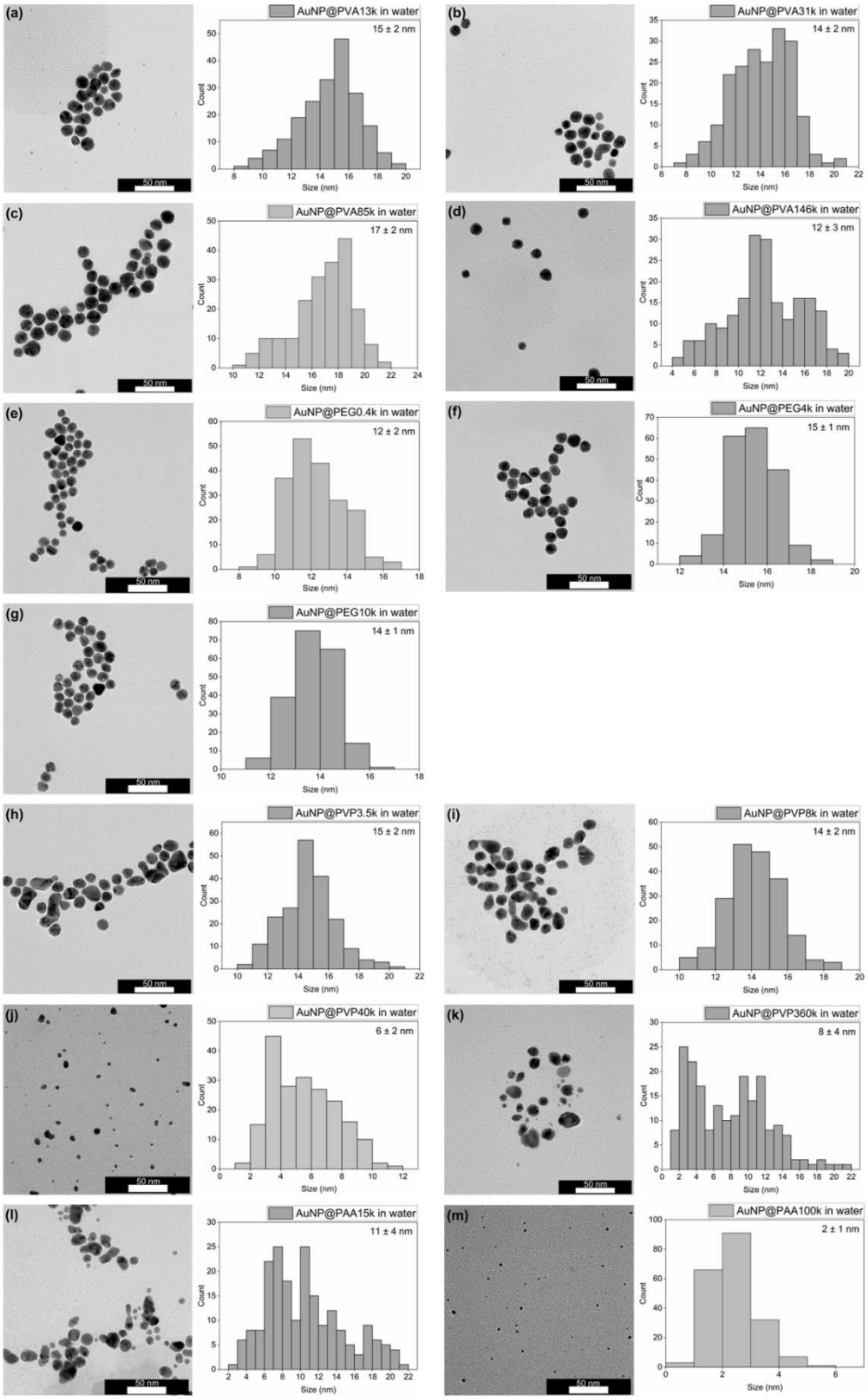

Figure 3. Representative TEM images and histograms (with the average size and its standard deviation given) of the one-pot synthesis in water of (**a**) AuNP@PVA13k (15 ± 2 nm), (**b**) AuNP@PVA31k (14 ± 2 nm), (**c**) AuNP@PVA85k (17 ± 2 nm), (**d**) AuNP@PVA146k (12 ± 3 nm), (**e**) AuNP@PEG0.4k (12 ± 2 nm), (**f**) AuNP@PEG4000 (15 ± 1 nm), (**g**) AuNP@PEG10k (14 ± 1 nm), (**h**) AuNP@PVP3.5k (15 ± 2 nm), (**i**) AuNP@PVP8k (14 ± 2 nm), (**j**) AuNP@PVP40k (6 ± 2 nm), (**k**) AuNP@PVP360k (8 ± 4 nm), (**l**) AuNP@PAA15k (11 ± 4 nm) and (**m**) AuNP@PAA100k (2 ± 1 nm). For the histograms 200 particles were analyzed using larger areas of the TEM images.

 doi:10.20944/preprints202508.0950.v1

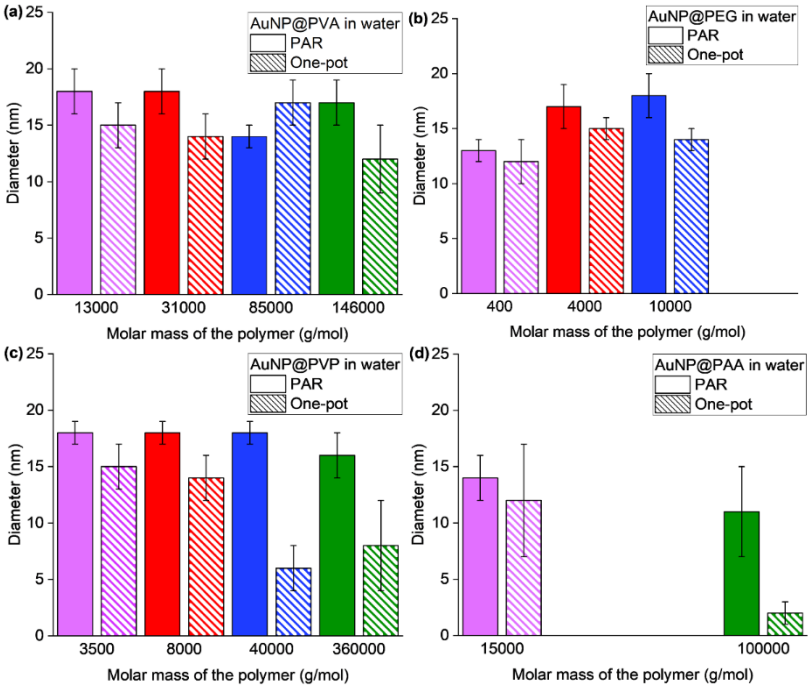

Figure 4. Overview of the TEM-derived AuNP core size and their standard deviation of the conjugates in water: (**a**) AuNP@PVA, (**b**) AuNP@PEG, (**c**) AuNP@PVP and (**d**) AuNP@PAA in water (fully colored bar PAR; hatched bar one-pot).

Direct and rapid size control of the dispersions is essential and TEM measurements are time consuming and require expensive instrumentation Consequently the samples were analyzed using dynamic light scattering (DLS). The DLS gives the hydrodynamic diameter (D_h) and the polydispersity of the AuNPs, taking into account the polymer coating and the solvate shell due to the solvent, both of which cannot be determined by TEM. Due to the polymer and solvent shell, the DLS data generally show larger size values than the TEM data [38]. For the AuNP@Polymer conjugates the hydrodynamic diameters from DLS have typically increased to 20-70 nm compared to gold core diameters of 11-18 nm (in water) from TEM (Table S1 and S2). From DLS the heterogeneity of the sample is given by the polydispersity index (PDI) which is a dimensionless parameter for the width of the particle size distribution in a sample. It is derived from the analysis of the autocorrelation function in the DLS and provides information on the heterogeneity of the particle sizes. A PDI value below 0.05 is typically an indicator of a monomodal dispersion. Values between 0.10 and 0.25 are characteristic of a narrow distribution, while values above 0.50 indicate a significantly broader distribution. At values above 0.70, the system has a very broad size distribution, which is rather unsuitable for DLS measurements [39–41]. The hydrodynamic diameters from DLS of the polymer-stabilized AuNPs in the water are given in Table S1 (together with the TEM diameters and the UV-Vis bands) and the DLS diagrams are shown in Figures S2-S17.

Figure 5 provides a summarizing overview of the DLS results and shows that D_h lies largely in the range of 20-70 nm for most samples, with the expected increase from the gold core size of 11-18 nm due to the polymer (and citrate) shell (Table S1). The one-pot method leads to a similar or higher D_h compared to the PAR method. However, for the polymer PVA, the D_h for the one-pot method also decreases for AuNP@PVA13k and AuNP@PVA146k compared to PAR. The D_h values are generally very similar for the AuNP@PEG samples and the samples with PVP8k and PVP40k. The PEG-based AuNPs show a relative constant D_h, independent of the polymer molar mass. A higher D_h by the one-pot method is then found for the AuNP conjugates with PVA31k and -85k, PVP3.5k and -360k and both PAA samples. The increase in D_h seen for the PVP- and PAA-based AuNPs from the one-pot synthesis could be caused by the non-spherical morphology of the AuNP cores which was visible in the TEM images. Non-spherical NPs can distort the results of the DLS measurements due to rotational

 doi:10.20944/preprints202508.0950.v1

movements and directional scattering, as the method is based on a spherical particle model. Anisotropic particles with different dimensions cannot be differentiated from each other in the DLS, as only an average hydrodynamic diameter is determined, which can deviate significantly from the actual particle dimensions. Although anisotropic particles may stand out in DLS due to a broad or multimodal size distribution, DLS does not provide accurate information about the particle shape [42]. It is again evident that the polymer functional groups, the chain length and mode of addition play a role in determining the AuNP@conjugate size with its hydrodynamic diameter. The effect of increasing or decreasing D_h does not only go in one direction when comparing the two synthesis methods of addition but can reverse for a given polymer with its chain length. The interfacial interaction between the growing AuNPs, the citrate and polymer shell plays a decisive role, resulting in different and competing surface coverage during the AuNP formation and growth. The general similarity of the hydrodynamic diameter of the PEG-based conjugates irrespective of polymer chain length which varies from 0.4k to 10k (in g/mol) may indicate little interaction of the PEG polymer with the AuNP@Cit surface. The more so as D_h for AuNP@Cit is 25 nm, close to the D_h values of 27, 27 and 32 nm for the three different AuNP@PEG conjugates (Table S1). This assumption of unperturbed AuNP@Cit particles in the presence of PEG is supported from their analysis in ethanol (see below).

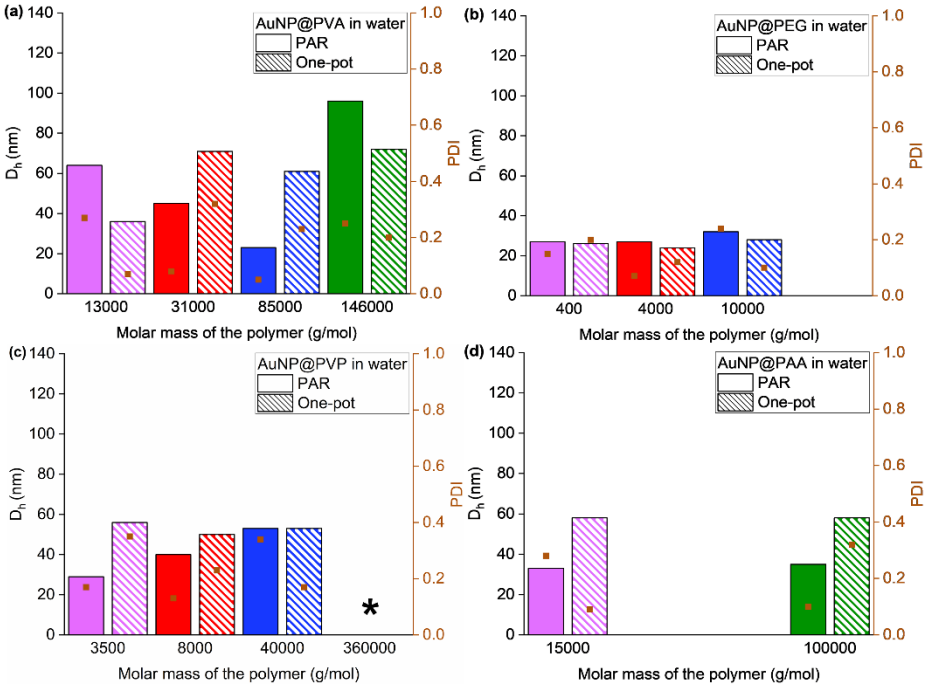

Figure 5. Graphical overview of all the DLS results in water of (**a**) AuNP@PVA, (**b**) AuNP@PEG, (**c**) AuNP@PVP and (**d**) AuNP@PAA (fully colored bar PAR; hatched bar one-pot). The brown squares represent the PDI. *The AuNP@PVP360k sample shows unexpectedly large hydrodynamic diameters for both the PAR method (177 nm) and the one-pot method (298 nm), which are off-scale.

The UV-Vis data overview in Figure 6 for the PAR method and Figure S10 for the one-pot method shows very similar absorption maxima for the surface plasmon resonance in the range from 517-to 525 nm and similar band width for most samples in water. The similarity in the absorption maxima and band width reflects the similar size of the AuNP cores from TEM analysis in the range of 11-18 nm and with small size dispersion. An exception is the surface plasmon resonances (SPR) of the samples AuNP@PAA15k and AuNP@PAA100K from the one-pot method in water, with a significant red shift of the maximum to 533 nm which correlates with the polydispersion seen in the TEM sample.

 doi:10.20944/preprints202508.0950.v1

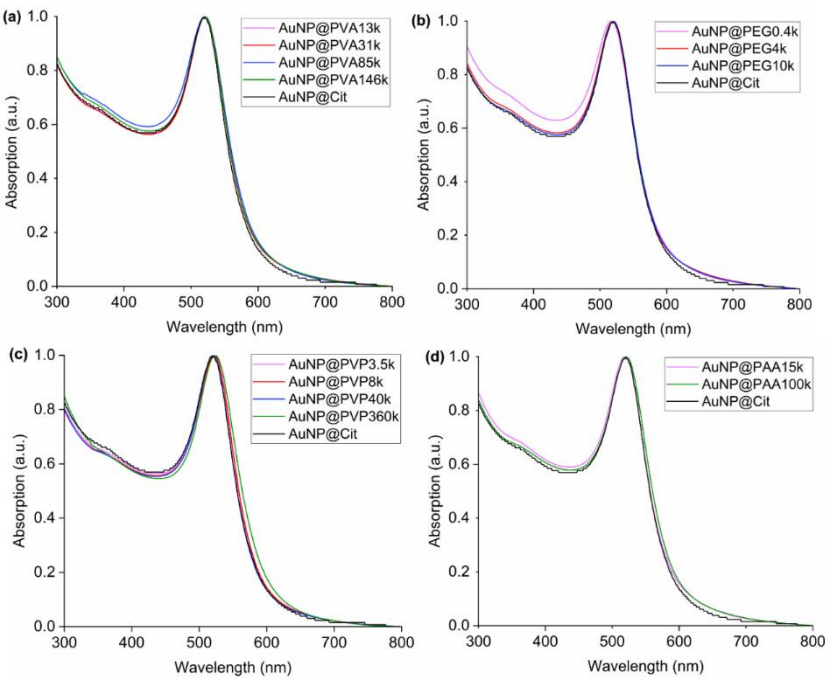

Figure 6. Ultraviolet-visible (UV-Vis) spectra in water from the PAR synthesis method of (**a**) AuNP@PVA, (**b**) AuNP@PEG, (**c**) AuNP@PVP and (**d**) AuNP@PAA. For the spectra from the one-pot method see Figure S10. The absorption maxima are listed in Table S1.

3.2. Characterization of the AuNP Samples Transferred to Ethanol

The TEM analysis in Figure 7, Figure S11 and S12 of the samples after their transfer into ethanol yields a range of 11-19 nm which is essentially identical to the 11-18 nm region of the samples in water. The numerical data of all samples in ethanol are listed in Table S2. Small changes such as an increase in size by a few nanometers, for example, for PAR AuNP@PVA85k, AuNP@PEG0.4k and AuNP@PAA100k, for one-pot AuNP@PVA13k, AuNP@PVA146k, AuNP@PEG0.4k and AuNP@PEG10k (Figure 7) should not be overinterpreted as this deviation is still within the standard deviation of 3σ. However, the samples prepared by the one-pot method with the polymers PVP and PAA100k showed no longer well-separated, individual AuNPs. Instead, these samples depicted highly aggregated, anisotropic and non-spherical nanoparticles. The non-spherical nature of the AuNPs with PVP and PAA100k from the one-pot method was already seen and noted in the TEM images in water, which were given in Figure 3, still there individual NPs could be discerned. Due to this heterogeneous appearance, a reliable particle diameter analysis in ethanol based on the TEM images was not possible. It is evident that the polymers PVP and PAA in combination with the one-pot synthesis are less stabilizing for AuNPs, especially when the nanoparticles are transferred from water to ethanol.

 doi:10.20944/preprints202508.0950.v1

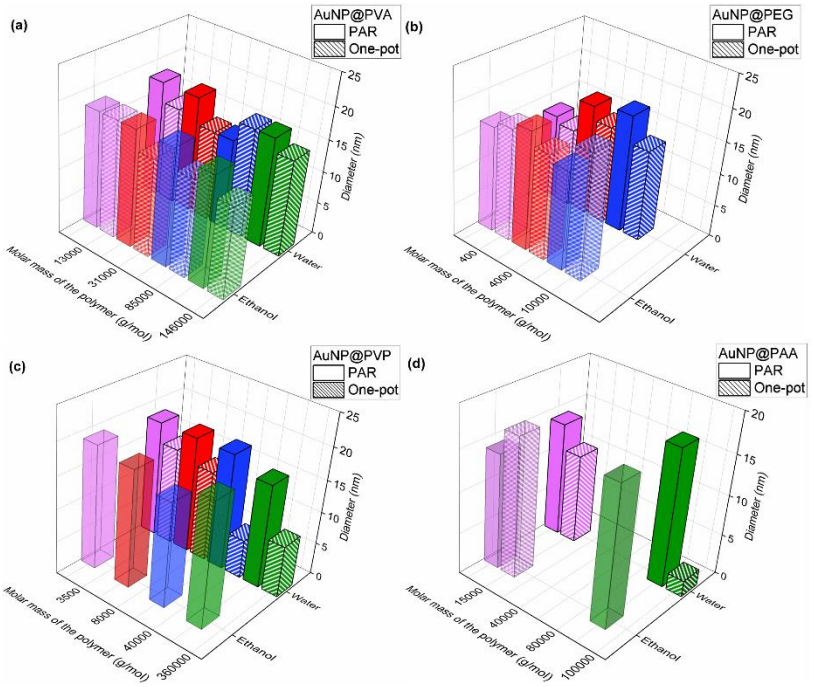

Figure 7. Graphical comparative overview of the TEM size in water and ethanol of (**a**) AuNP@PVA, (**b**) AuNP@PEG, (**c**) AuNP@PVP and (**d**) AuNP@PAA (fully colored bar PAR; hatched bar one-pot). The individual TEM images for the ethanol samples are given in Figure S11 and S12, numerical data of the samples in ethanol is listed in Table S2. The bars for the ethanol dispersion are shown transparent so that the bars in the water row can be seen more clearly.

The comparative overview of the hydrodynamic diameter from DLS in water and ethanol in Figure 8 indicates the expected increase in D_h with increasing molar mass of the polymer. It can be concluded not only from TEM but also from DLS and UV-Vis (Figure 8, Figure S22 and S23) that the nanoparticles from the PAR method remain rather unperturbed when transferred from water to ethanol. A single exception are the PEG10k-coated NPs. Here DLS data in ethanol show a hydrodynamic diameter of 163 nm (vs 32 nm in water) and a strong red-shift to 699 nm can be witnessed in the UV-Vis spectra (vs 520 nm in water) (cf. Table S2 and Table S1). Perhaps this aggregation deduced from the solution methods DLS and UV-Vis of the AuNP@PEG10k conjugates could be inferred also from the TEM image in Figure S11 where the individual gold cores are very close together, much closer than in the TEM images with the other polymers. This proximity where the nanoparticles appear to touch each other could derive from a missing polymer coating, that is washed away. In the discussion of the DLS analysis in water we had already noted that the very similar hydrodynamic diameter of the PEG-based conjugates, irrespective of polymer chain length, may indicate little interaction of the PEG polymer with the gold core.

 doi:10.20944/preprints202508.0950.v1

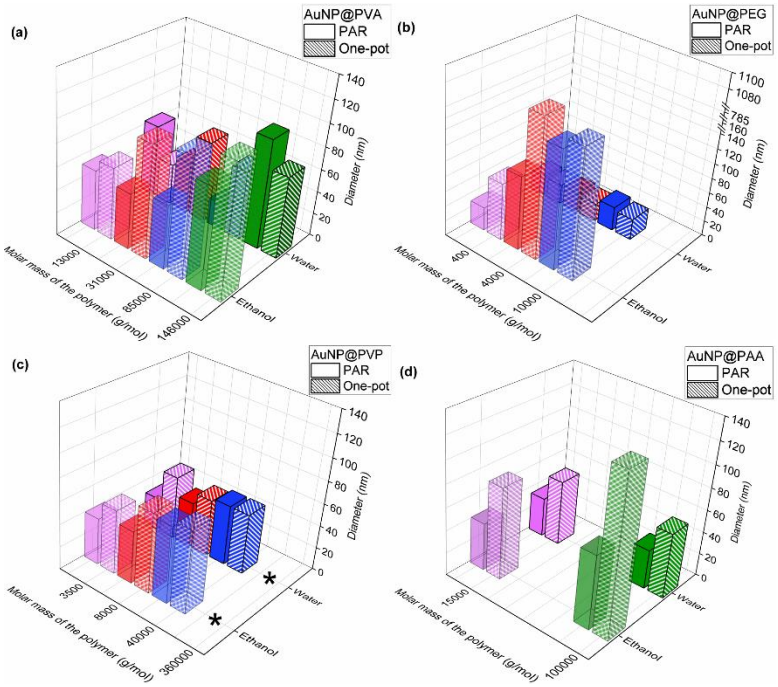

Figure 8. Comparative overview of the hydrodynamic diameter from DLS in water and ethanol of (**a**) AuNP@PVA, (**b**) AuNP@PEG, (**c**) AuNP@PVP and (**d**) AuNP@PAA (fully colored bar PAR; hatched bar one-pot). Note the split diameter axis for the PEG samples. The individual DLS images for the ethanol samples are given in Figure S14-S21 and S22, numerical data of the samples in ethanol is listed in Table S2. The bars for the ethanol dispersion are shown transparent so that the bars in the water row can be seen more clearly. *The AuNP@PVP360k samples show unexpectedly large hydrodynamic diameters (Table S1 and S2), which are off-scale.

The nanoparticle instability from the one-pot synthesis with the polymers PVP and PAA100k, which was evident in the TEM images (compare Figure 3 and Figure S12), was not immediately evident in the DLS analysis of the PVP samples where the hydrodynamic diameter in ethanol remained similar to those measured in water (Figure 8 and Figure S22). Yet, in the UV-Vis spectra in ethanol there is a broadening of the bands for AuNP@PVP, especially evident for PVP3.5k and PVP360k with also a bathochromic shift to 531 nm and more significant to 576 nm for PVP360k (Figure S24). From the one-pot synthesis the longer-chain PEG conjugates exhibit a very large increase in hydrodynamic diameter in DLS after their transfer into ethanol (Figure 8). For UV-Vis and AuNP@PEG10k the same strong red-shift as with PAR is seen in the one-pot product (Figure S23 and Figure S24). For PAA100k the hydrodynamic diameter increased in ethanol to 139 nm (vs 58 nm in water) (cf. Table S2 and Table S1) and the UV-Vis band strongly broadened (Figure S24).

For the AuNPs functionalized with PEG a tendency towards instability in ethanol can be inferred from the DLS and UV-Vis measurements. This is due to the comparatively weak interaction of PEG with the AuNP surface, since PEG contains only ether groups that do not have a strong binding affinity to gold. Furthermore, nonpolar PEG provides largely a steric stabilization, whereas the more polar PVA, PVP and PAA polymers enable also some electrostatic stabilization. Further, the high solubility of PEG in ethanol, also adds to its removal from the nanoparticle surface, leaving only the citrate layer, if any, and thus contributes to the tendency of the gold cores to aggregate [43–45]. Of all the polymers used in both synthesis methods, the PVA-coated AuNPs exhibit the highest colloidal stability both in water and after transfer to ethanol.

Overall, the AuNP@Polymer conjugates show less stabilization in ethanol than in water, also because highly polar water has a high dielectric constant (approx. 80), which gives stronger electrostatic interactions and can shield charges more efficiently. The dielectric constant of less polar ethanol is only about 25, which means that the electrostatic shielding is weaker and the particles can attract each other and agglomerate [46,47]. Water also builds a stable hydrogen bond network to

 doi:10.20944/preprints202508.0950.v1

polymer chains with H-bond acceptors (OH in PVA, N-CO in PVP and CO_2^- in PAA), which then can be solvated effectively. In ethanol, a weaker hydrogen bonding network is formed, so that the polymer shells of the AuNP@Polymer conjugates can approach and interact better, which results in their aggregation in solution [48–52].

3.3. Loading of DASA on the AuNP@Polymer Conjugates

As a test for drug loading, we have investigated here the loading of the tyrosine kinase inhibitor (TKI) Dasatinib (BMS-354825, Sprycel®) (DASA) for which the solvent needed to be changed to ethanol as DASA is not soluble in water but, e.g., in ethanol.

DASA (see Scheme S1 for the molecular structure) can be used as a drug to treat cancer and against drug resistance [53]. It inhibits the phosphorylation of the oncogenic and Src kinase families and can thus prevent angiogenesis and the associated tumor growth and support apoptosis [32,54,55]. As a TKI, it can be used in many tumor types such as leukemia, glioblastoma multiforme (GBM), pancreatic ductal adenocarcinoma (PDAC) and many others [56–59].

To determine the mass loading of DASA per mass of gold, the combined DASA and AuNP@Polymer dispersions (volume 5.8 mL) were stirred and centrifuged after 72 h. The supernatants were removed with a pipette and stored in the refrigerator at 4 °C until the HPLC measurement was performed. From the HPLC measurement the remaining DASA concentration was determined with the calibration curve in Figure S25. From the difference to the starting concentration of DASA the mass which was adsorbed on the AuNP@Polymer conjugate was obtained.

A typical DASA loading was in the range of 100-300 µg/mg of gold for all polymers except for PVA for both the PAR and one-pot method samples. For the PVA samples the loading was consistently below 100 µg/mg and often close to no loading at all. There may be some correlation of the DASA loading for the PEG, PVP and PAA conjugates with their observed tendency of aggregation in ethanol as discussed above.

4. Conclusions

AuNP@Polymer conjugates were prepared in water by two different synthesis methods using polymers with different functional groups and chain lengths to compare their eligibility to stabilize the nanoparticles in water and ethanol. The gold precursor $KAuCl_4$ was reduced to Au(0) with sodium citrate. The polymers were either post-synthetically added (PAR) or were already present during the reduction in a one-pot method. Stable conjugates in water could be produced with all AuNP polymer systems using both PAR and one-pot. Characterization by TEM and DLS yield similar gold core sizes of 11-18 in water or 11-19 nm in ethanol, and hydrodynamic diameters of 20-70 nm for most AuNP@Polymer samples and both synthesis methods and solvents. Among all polymers tested, PVA showed the highest colloidal stability in both aqueous and ethanolic environments, regardless of the synthesis route, and was therefore most effective in preventing the aggregation of AuNPs. When the samples were transferred from water to ethanol some aggregation of the nanoparticles became apparent generally for the PEG coated particles and for PVP and PAA dependent on their molecular weight and synthesis combination. The obvious lower stabilizing effect of the PEG polymers may be due to the less coordinating ether groups. The AuNP@Polymer conjugates could be successfully loaded with the anticancer drug DASA for the PEG, PVP and PAA polymers. For future work polymers with better coordinating groups, such as thiol groups should be used, as gold has a high affinity for thiolated molecules, for example Thio-PEG or Thio-PVA. These polymers bind to the AuNP surface via an S-linker and can enable a more stable polymer shell. Hydrophobic polymers such as poly(lactide-co-glycolide) could also be tested towards hydrophobic drug loading. Future works on the stabilizing effect of different polymers should also focus on the colloidal stability of AuNPs in complex biological media under physiologically relevant cell culture media conditions.

 doi:10.20944/preprints202508.0950.v1

Supplementary Materials: The following supporting information can be downloaded at: https://www.mdpi.com/article/doi/s1, Section S1. Characterization of AuNP@Cit and AuNP@Polymer in water.; Section 2. Characterization of AuNP@Polymer in ethanol after transfer from water; Section S3. Quantification of DASA loading.

Author Contributions: Conceptualization, M.K., A.Y.S, U.D.K.; methodology, M.K.; software, M.K.; validation, M.K.; formal analysis, M.K.; investigation, M.K. and R.L.V.; resources, C.J.; data curation, M.K.; writing—original draft preparation, M.K.; writing—review and editing, M.K., A.Y.S., U.D.K. and C.J.; visualization, M.K.; supervision, C.J.; project administration, C.J.; funding acquisition, C.J. All authors have read and agreed to the published version of the manuscript.

Funding: Bundesamt für Strahlenschutz (FKZ 3622S7229B, Integrated molecular Imaging for Personalized Biomarker-based Breast Cancer Characterization and Treatment, IMMPRINT).

Institutional Review Board Statement: Not applicable

Informed Consent Statement: Not applicable

Data Availability Statement: The original contributions presented in this study are included in the article/Supplementary Materials. Further inquiries can be directed to the corresponding author.

Acknowledgments: The authors would like to thank the Core Facility for Electron Microscopy of the Institute of Medical Faculty of the Heinrich Heine University Düsseldorf for access to the JEOL JEM-2100Plus electron microscope instrument.

Conflicts of Interest: The authors declare no conflicts of interest.

Abbreviations

The following abbreviations are used in this manuscript:

AuNPs	Gold nanoparticles
PAR	Postsynthetic addition reaction
PVA	Poly(vinyl alcohol)
PEG	Poly(ethylene glycol)
PVP	Poly(vinyl pyrrolidone)
PAA	Poly(acrylic acid)
TEM	Transmission electron microscopy
DLS	Ultraviolet-visible spectroscopy
HPLC	High-performance liquid chromatography
NaCit	Sodium citrate dihydrate
PDI	Polydispersity index
DASA	Dasatinib

References

1. Liang, M.; Lin, I.-C.; Whittaker, M.R.; Minchin, R.F.; Monteiro, M.J.; Toth, I. Cellular Uptake of Densely Packed Polymer Coatings on Gold Nanoparticles. *ACS Nano* **2010**, *4 (11)*, 403-413, https://doi.org/10.1021/nn9011237.
2. Richards, S.-J.; Gibson, M.I. Optimization of the Polymer Coating for Glycosylated Gold Nanoparticle Biosensors to Ensure Stability and Rapid Optical Readouts. *ACS Macro Lett.* **2014**, *3 (10)*, 1004-1008, https://doi.org/10.1021/mz5004882.
3. Silva, V.C.J.D.; Silva, R.N.O.; Colli, L.G.; Carvalho, M.H.C.; Rodrigues, S.F. Gold nanoparticles carrying or not anti-VEGF antibody do not change glioblastoma multiforme tumor progression in mice. *Heliyon* **2020**, *6 (11)*, https://doi.org/10.1016/j.heliyon.2020.e05591.
4. Kang, J.H.; Cho, J.; Ko, Y.T. Investigation on the effect of nanoparticle size on the blood-brain tumor barrier permeability by *in situ* perfusion via internal carotid artery in mice. *J. Drug Target.* **2018**, *27 (1)*, 103-110, https://doi.org/10.1080/1061186X.2018.1497037.

 doi:10.20944/preprints202508.0950.v1

5. Chen, Y.; Feng, X. Gold nanoparticles for skin drug delivery. *Int. J. Pharm.* **2022**, *625*, 122122, https://doi.org/10.1016/j.ijpharm.2022.122122.
6. Nejati, K.; Dadashpour, M., Gharibi, T.; Mellatyar, H.; Akbarzadeh, A. Biomedical Applications of Functionalized Gold Nanoparticles: A Review. *J. Clust. Sci.* **2022**, *33*, 1–16, https://doi.org/10.1007/s10876-020-01955-9.
7. Sani, A.; Cao, C.; Cui, D. Toxicity of gold nanoparticles (AuNPs): A review. *Biochem. Biophys. Rep.* **2021**, *26*, 100991, https://doi.org/10.1016/j.bbrep.2021.100991.
8. Kesharwani, P., Ma, R., Sang, L.; Fatima, M.; Sheikh, A.; Abourehab, M.A.S.; Gupta, N.; Chen, Z.-S.; Zhou, Y. Gold nanoparticles and gold nanorods in the landscape of cancer therapy. *Mol Cancer* **2023**, *22 (98),* https://doi.org/10.1186/s12943-023-01798-8.
9. Jain, P.K.; Lee, K.S.; El-Sayed, I.H.; El-Sayed, M.A. Calculated Absorption and Scattering Properties of Gold Nanoparticles of Different Size, Shape, and Composition: Applications in Biological Imaging and Biomedicine. *J. Phys. Chem. B* **2006**, *110 (14)*, 7238-7248, https://doi.org/10.1021/jp057170o.
10. Huang, X.; El-Sayed, I.H.; Qian, W.; El-Sayed, M.A. Cancer Cell Imaging and Photothermal Therapy in the Near-Infrared Region by Using Gold Nanorods. *J. Am. Chem. Soc.* **2006**, *128 (6)*, 2115-2120, https://doi.org/10.1021/ja057254a.
11. Ghobashy, M.M.; Alkhursani, S.A.; Alqahtani, H.A.; El-damhougy, T.K.; Madani, M. Gold Nanoparticles in microelectronics advancements and biomedical applications. *Mater. Sci. Eng. B* **2024**, *301*, 117191, https://doi.org/10.1016/j.mseb.2024.117191.
12. Hussain, M.H.; Abu Bakar, N.F.; Mustapa, A.N.; Low, K.-F.; Othman, N.H.; Adam, F. Synthesis of Various Size Gold Nanoparticles by Chemical Reduction Method with Different Solvent Polarity. *Nanoscale Res Lett*. **2020**, *15 (140)*, https://doi.org/10.1186/s11671-020-03370-5.
13. Aboudzadeh, M.A.; Kruse, J.; Iglesias, M.S.; Cangialosi, D.; Alegria, A.; Grzelczak, M.; Barroso-Bujans, F. Gold nanoparticles endowed with low-temperature colloidal stability by cyclic polyethylene glycol in ethanol. *Soft Matter*. **2021**, *17 (33)*, 7792-7801, https://doi.org/10.1039/D1SM00720C.
14. Reznickova, A.; Slepicka, P.; Slavikova, N.; Staszek, M.; Svorcik, V. Preparation, aging and temperature stability of PEGylated gold nanoparticles. *Colloid. Surf. A* **2017**, *523*, 91-97, https://doi.org/10.1016/j.colsurfa.2017.04.005.
15. Tsutsui, G.; Huang, S.; Sakaue, H.; Shingubara, S.; Takahagi, T. Well-size-controlled Colloidal Gold Nanoparticles Dispersed in Organic Solvents. *Jpn. J. Appl. Phys.* **2001**, *40*, 346-349, **https://doi.org/10.1143/JJAP.40.346**.
16. Chowdhury, P.; Chaki, S.; Sen, A.; Dasgupta, S. Cataractous Eye Protein Isolate Stabilized Gold Nanoparticles Prevent Their Ethanol-Induced Aggregation. *J. Phys. Chem. B* **2024**, *129 (7)*, 1934-1945, https://doi.org/10.1021/acs.jpcb.4c07076.
17. Sen, G.T.; Ozkemahli, G.; Shahbazi, R.; Erkekoglu, P.; Ulubayram, K.; Kocer-Gumusel, B. The Effects of Polymer Coating of Gold Nanoparticles on Oxidative Stress and DNA Damage. *Int. J. Toxicol*. **2020**, *39 (4)*, 328-340, https://doi.org/10.1177/1091581820927646.
18. Albanese A, Chan W.C. Effect of gold nanoparticle aggregation on cell uptake and toxicity. *ACS Nano* **2011**, *5 (7)*, 5478-89, https://doi.org/10.1021/nn2007496.
19. Qiu, Y.; Liu, Y.; Wang, L.; Xu, l.; Bai, R.; Ji, Y.; Wu, X.; Zhao, Y.; Li, Y.; Chen, C. Surface chemistry and aspect ratio mediared cellular uptake of Au nanorods. *Biomaterials* **2010**, *31*, 7606-7619. https://doi.org/10.1016/j.biomaterials.2010.06.051
20. Anniebell, S.; Gopinath, S.C.B. Polymer Conjugated Gold Nanoparticles in Biomedical Applications. *Curr. Med. Chem.* **2018**, *25 (12)*, 1433-1445, https://doi.org/10.2174/0929867324666170116123633.
21. Hecold, M.; Buczkowska, R.; Mucha, A.; Grzesiak, J.; Rac-Rumijowska, O.; Teterycz, H.; Marycz, K. The Effect of PEI and PVP-Stabilized Gold Nanoparticles on Equine Platelets Activation: Potential Application in Equine Regenerative Medicine. *J. Nanomater.* **2017**, *1*, 8706921, https://doi.org/10.1155/2017/8706921.
22. Retout, M.; Blond, P.; Jabin, I.; bruylants, G. Ultrastable PEGylated Calixarene-Coated Gold Nanoparticles with a Tunable Bioconjugation Density for Biosensing Applications. *Bioconjugate Chem.* **2021**, *32 (2)*, 290-300, https://doi.org/10.1021/acs.bioconjchem.0c00669.

 doi:10.20944/preprints202508.0950.v1

23. Zhang, X.; Guo, X.; Kang, X.; Yang, H.; Guo, W.; Guan, L.; Wu, H.; Du, L. Surface Functionalization of Pegylated Gold Nanoparticles with Antioxidants Suppresses Nanoparticle-Induced Oxidative Stress and Neurotoxicity. *Chem. Res. Toxicol.* **2020**, *33 (5)*, 1195-1205, https://doi.org/10.1021/acs.chemrestox.9b00368.
24. Kozics, K.; Sramkova, M.; Kopecka, K.; Begerova, P.; Manova, A.; Krivosikova, Z.; Sevcikova, Z.; Liskova, A.; Rollerova, E.; Dubaj, T.; Puntes, V.; Wsolova, L.; Simon, P.; Tulinska, J.; Gabelova, A. Pharmacokinetics, Biodistribution, and Biosafety of PEGylated Gold Nanoparticles In Vivo. *Nanomaterials* **2021**, *11*, 1702, https://doi.org/10.3390/nano11071702.
25. Pedziwiatr-Werbicka, E.; Gorzkiewicz, M.; Horodecka, K.; Lach, D.; Barrios-Gumiel, A.; Sánchez-Nieves, J.; Gómez, R.; de la Mata, F.J.; Bryszewska, M. PEGylation of Dendronized Gold Nanoparticles Affects Their Interaction with Thrombin and siRNA. *J. Phys. Chem. B* **2021**, *125*, 1196–1206, https://doi.org/10.1021/acs.jpcb.0c10177.
26. Soares, S.; Faria, I.; Aires, F.; Monteiro, A.; Pinto, G.; Sales, M.G.; Correa-Duarte, M.A.; Guerreiro, S.G.; Fernandes, R. Application of Gold Nanoparticles as Radiosensitizer for Metastatic Prostate Cancer Cell Lines. *Int. J. Mol. Sci.* **2023**, *24*, 4122, https://doi.org/10.3390/ijms24044122.
27. Nguyenova, H.Y.; Kalbacova, M.H.; Dendisova, M.; Sikorova, M.; Jarolimkova, J.; Kolska, Z.; Ulrychova, L.; Weber, J.; Reznickova, A. Stability and biological response of PEGylated gold nanoparticles. *Heliyon* **2024**, *10* (9), https://doi.org/10.1016/j.heliyon.2024.e30601.
28. Shan, Y.; Ma, S.; Nie, L.; Shang, X.; Hao, X.; Tang, Z.; Wang, H. Size-dependent endocytosis of single gold nanoparticles. *Chem. Commun.* **2011**, *47*, 8091-8093, https://doi.org/10.1039/C1CC11453K.
29. Qiu, Y.; Liu, Y.; Wang, L.; Xu, L.; Bai, R.; Ji, Y.; Wu, X.; Zhao, Y.; Li, Y.; Chen. C. Surface chemistry and aspect ration mediated cellular uptake of Au nanorods. *Biomaterials* **2010**, *31 (30)*, 7606-19, https://doi.org/10.1016/j.biomaterials.2010.06.051.
30. Yang, Y.; Zheng, X.; Chen, L.; Gong, X.; Yang, H.; Duan, X.; Zhu, Y. Multifunctional Gold Nanoparticles in Cancer Diagnosis and Treatment. *Int. J. Nanomed.* **2022**, *17*, 2041-2067, https://doi.org/10.2147/IJN.S355142.
31. Giesen, B.; Nickel, A.-C.; Barthel, J.; Kahlert, U.D.; Janiak, C. Augmented Therapeutic Potential of Glutaminase Inhibitor CB839 in Glioblastoma Stem Cells Using Gold Nanoparticle Delivery. *Pharmaceutics* **2021**, *13*, 295, https://doi.org/10.3390/pharmaceutics13020295.
32. Kaul, M.; Sanin, A.Y.; Shi, W.; Janiak, C.; Kahlert, U.D. Nanoformulation of dasatinib cannot overcome therapy resistance of pancreatic cancer cells with low LYN kinase expression. *Pharmacol. Rep.* **2024**, *76*, 793–806, https://doi.org/10.1007/s43440-024-00600-w.
33. Chechiek, V. Reduced Reactivity of Aged Au Nanoparticles in Ligand Exchange Reactions. *J. Am. Chem. Soc.* **2004**, *126 (25)*, 7780-7781, https://doi.org/10.1021/ja048879w.
34. Woehrle, G.H.; Brown, L.O.; Hutchison, J.E. Thiol-Functionalized, 1.5-nm Gold Nanoparticles through Ligand Exchange Reactions: Scope and Mechanism of Ligand Exchange. *J. Am. Chem. Soc.* **2005**, *127 (7)*, 2172-2183, https://doi.org/10.1021/ja0457718.
35. Ishida, Y.; Suzuki, J.; Akita, I.; Yonezawa, T. Ultrarapid Cationization of Gold Nanoparticles via a Single-Step Ligand Exchange Reaction. *Langmuir* **2018**, *34 (36)*, 10668-10672, https://doi.org/10.1021/acs.langmuir.8b02226.
36. Turkevich, J.; Stevenson, P.C.; Hillier, J. A study of the nucleation and growth processes in the synthesis of colloidal gold. *Discuss. Faraday Soc.* **1951**, *11*, 55-75, https://doi.org/10.1039/df9511100055.
37. Shimmin, R.G.; Schoch, A-B.; Braun, P.V. Polymer Size and Concentration Effects on the Size of Gold Nanoparticles Capped by polymeric Thiols. *Langmuir* **2004,** *20 (13)*, 5613-5620, https://doi.org/10.1021/la036365p.
38. Tomaszewska, E.; Soliwoda, K.; Kadziola, K.; Tkacz-Szczesna, B.; Celichowski, G.; Cichomski, M.; Szmaja, W.; Grobelny, J. Detection Limits of DLS and UV-Vis Spectroscopy in Characterization of Polydisperse Nanoparticles Colloids. *J. Nanomater.* **2013**, *1*, 313081, https://doi.org/10.1155/2013/313081.
39. Gharib, R.; Greige-Gerges, H.; Fourmentin, S.; Charcosset, C. Hydroxypropyl-ß-cyclodextrin as a membrane protectant during freeze-drying of hydrogenated and non-hydrogenated liposomes and molecule-in-cyclodextrin-in- liposomes: Application to trans-anethole. *Food Chem.* **2018**, *267*, 67-74, https://doi.org/10.1016/j.foodchem.2017.10.144.

 doi:10.20944/preprints202508.0950.v1

40. Danaei, M.; Dehghankhold, M.; Ataei, S.; Hasanzadeh Davarani, F.; Javanmard, R.; Dokhani, A.; Khorasani, S.; Mozafari, M.R. Impact of Particle Size and Polydispersity Index on the Clinical Applications of Lipidic Nanocarrier Systems. *Pharmaceutics* **2018**, *10 (2)*, 57, https://doi.org/10.3390/pharmaceutics10020057.
41. Hoseini, B.; Jaafari, M.R.; Golabpour, A.; Momtazi-Borojeni, A.A.; Karimi, M.; Eslami, S. Application of ensemble machine learning approach to assess the factors affecting size and polydispersity index of liposomal nanoparticles. *Sci. Rep.* **2023**, *13 (1)*, 18012, https://doi.org/10.1038/s41598-023-43689-4.
42. Feller, D.; Otten, M.; Hildebrandt, M.; Krüsmann, M.; Bryant, G.; Karg, M. Translational and rotational diffusion coefficients of gold nanorods functionalized with a high molecular weight, thermoresponsive ligand: a depolarized dynamic light scattering study. *Soft Matter* **2021**, *17*, 4019, https://doi.org/10.1039/D1SM00077B.
43. Zhang, X.; Jimmy Huang, P.-J.; Servos, M.R.; Liu, J. Effects of Polyethylene Glycol on DNA Adsorption and Hybridization on Gold Nanoparticles and Graphene Oxide. *Langmuir* **2012**, *28*, 14330-14337, https://doi.org/10.1021/la302799s.
44. Uz, M.; Bulmus, V.; Altinkaya, S.A. Effect of PEG Grafting Density and Hydrodynamic Volume on Gold Nanoparticle−Cell Interactions: An Investigation on Cell Cycle, Apoptosis, and DNA Damage. *Langmuir* **2016**, *32*, 5997-6009, https://doi.org/10.1021/acs.langmuir.6b01289.
45. Chen, H.; Paholak, H.; Ito, M.; Sansanaphongpricha, K.; Qian, W.; Che, Y.; Sun, D. 'Living' PEGylation on gold nanoparticles to optimize cancer cell uptake by controlling targeting ligand and charge densities. *Nanotechnology* **2013**, *24*, 355101, https://doi.org/10.1088/0957-4484/24/35/355101.
46. Mohsen-Nia, M.; Amiri, H.; Jazi, B. Dielectric Constants of Water, Methanol, Ethanol, Butanol and Acetone: Measurement and Computational Study. *J. Solution Chem.* **2010**, *39*, 701-708, https://doi.org/10.1007/s10953-010-9538-5.
47. Tseng, K.-H.; Liao, C.-Y.; Huang, J.-C.; Tien, D.-C.; Tsung, T.-T. Characterization of gold nanoparticles in organic or inorganic medium (ethanol/water) fabricated by spark discharge method. *Mater. Lett.* **2008**, *62 (19)*, 3341-3344, https://doi.org/10.1016/j.matlet.2008.02.056.
48. Liao, J.; Zhang, Y.; Yu, W.; Xu, L.; Ge, C.; Liu, J.; Gu, N. Linear aggregation of gold nanoparticles in ethanol. Colloids and Surfaces A: Physicochem. *Colloids Surf. A Physicochem. Eng. Asp.* **2003**, *223 (1-3)*, 177-183, https://doi.org/10.1016/S0927-7757(03)00156-0.
49. Tilaki, R.M.; Iraji zad, A.; Mahdavi, S.M. The effect of liquid environment on size and aggregation of gold nanoparticles prepared by pulsed laser ablation. *J. Nanopart. Res.* **2007**, *9*, 853-860, https://doi.org/10.1007/s11051-006-9143-0.
50. Lu, H.; Huang, W.M.; Fu, Y.Q.; Leng, J. Quantitative separation of the influence of hydrogen bonding of ethanol-water mixture on the shape recovery behavior of polyurethane shape memory polymer. *Smart Mater. Struct.* **2014**, *23*, 125041, https://doi.org/10.1088/0964-1726/23/12/125041.
51. Jewrajka, S.K.; Chatterjee, U. Block copolymer mediated synthesis of amphiphilic gold nanoparticles in water and an aqueous tetrahydrofuran medium: An approach for the preparation of polymer–gold nanocomposites. *J. Polym. Sci., Part A: Polym. Chem.* **2006**, *44 (6)*, 1841-1854, https://doi.org/10.1002/pola.21293.
52. Mani, S.; Khabaz, F.; Godbole, R.V.; Hedden, R.C.; Khare, R. Structure and Hydrogen Bonding of Water in Polyacrylate Gels: Effects of Polymer Hydrophilicity and Water Concentration. *J. Phys. Chem. B.* **2015**, *119 (49)*, 15381-15393, https://doi.org/10.1021/acs.jpcb.5b08700.
53. Galanis, E.; Anderson, S.K., Twohy, E.L.; Carrero, X.W.; Dixon, J.G.; Tran, D.D.; Jeyapalan, S.A.; Anderson, D.M.; Kaufmann, T.J.; Feathers, R.W.; Giannini, C.; Buckner, J.C.; Anastasiadis, P.Z.; Schiff, D. A phase 1 and randomized, placebo-controlled phase 2 trial of bevacizumab plus dasatinib in patients with recurrent glioblastoma: Alliance/North Central Cancer Treatment Group N0872. *Cancer* **2019**, *125 (21)*, 3790-3800, https://doi.org/10.1002/cncr.32340.
54. Gnoni, A.; Marech, I.; Silvestris, N.; Vacca, A.; Lorusso, V. Dasatinib: an anti-tumour agent via Src inhibition. *Curr. Drug Targets* **2011**, *12*, 563-578, https://doi.org/10.2174/138945011794751591.
55. Usama, S.M.; Jiang, Z.; Pflug, K.; Sitcheran, R.; Burgess, K. Conjugation of Dasatinib with MHI-148 Has a Significant Advantageous Effect in Viability Assays for Glioblastoma Cells. *ChemMedChem* **2019**, *14 (17)*, 1575-1579, https://doi.org/10.1002/cmdc.201900356.

 doi:10.20944/preprints202508.0950.v1

56. Dumont, R.A.; Hildebrandt, I.; Su, H.; Haubner, R.; Reischl, G.; Czernin, J.G.; Mischel, P.S.; Weber, W.A. Noninvasive imaging of alphaVbeta3 function as a predictor of the antimigratory and antiproliferative effects of dasatinib. *Cancer Res*. **2009**, *69 (7)*, 3173-3179, https://doi.org/10.1158/0008-5472.CAN-08-3390.
57. de Groot, J.; Milano, V. Improving the prognosis for patients with glioblastoma: the rationale for targeting Src. *J. Neurooncol.* **2009**, *95 (2)*, 151-163, https://doi.org/10.1007/s11060-009-9916-2.
58. Teng, T.; Cai, Y.; Pi, W.; Gao, L.; Shay, C. Augmentation of the anticancer activity of CYT997 in human prostate cancer by inhibiting Src activity. *J. Hematol. Oncol*. **2017**, *10 (1)*, 118, https://doi.org/10.1186/s13045-017-0485-0.
59. Rice, L.; Lepler, S.; Pampo, C.; Siemann, D.W. Impact of the SRC inhibitor dasatinib on the metastatic phenotype of human prostate cancer cells. *Clin. Exp. Metastasis* **2012**, *29 (2)*, 133-142, https://doi.org/10.1007/s10585-011-9436-2.